Korean J. Chem. Eng., 39(11), 3155-3164 (2022)
DOI: 10.1007/s11814-022-1164-6

pISSN: 0256-1115
eISSN: 1975-7220

Efficient dual adsorption of eosinY and methylene blue from aqueous solution using nanocomposite of graphene oxide nanosheets and ZnO nanospheres

Nisar Ahmad*, Samina Karim*, Dilshad Hussain*, Young Sun Mok,†, and Ghayas Uddin Siddiqui*,**,†**

*H.E.J. Research Institute of Chemistry, International Center for Chemical and Biological Sciences, University of Karachi, Karachi, Pakistan
**Department of Chemical and Biological Engineering, Jeju National University, Jeju 63243, Korea
(*Received 13 January 2022 • Revised 22 April 2022 • Accepted 30 April 2022*)

Abstract−A versatile graphene oxide nanosheets-ZnO nanospheres nanocomposite was synthesized for removal of dyes via adsorption process and characterized by various techniques, such as X-ray diffraction (XRD), Scanning electron microscopy (SEM), Fourier transform infrared (FTIR), and zeta potential (ZP) analyzer. The synthesized nanocomposite (NCs) was utilized as an efficient adsorbent for the removal of anionic dye eosin y (EY) as well as cationic dye methylene blue (MB) from aqueous solutions. The kinetics of adsorption was studied by pseudo-first and pseudo-second-order kinetics and the adsorption data was well in agreement with the pseudo-second-order model. The R^2 values of 0.9971 and 0.9839 of the second order for EY and MB, respectively, were greater than that of the first order. To calculate the most suitable isotherm model for adsorption, the Freundlich and Langmuir isotherms were applied and the data for both dyes fitted well with the Langmuir model. The maximum adsorption capacities obtained from Langmuir isotherm for EY and MB were 555.55 and 250 mg/g, respectively. Remarkably, 3.0 mg/13 mL of nanocomposite adsorbed 0.1 mg/mL of EY and 0.04 mg/mL of MB in the very short time of 10 and 15 minutes, respectively. The high adsorption efficiency of GO/ZnO NCs suggests that they may be a useful adsorbent for the purification of industrial wastewater.

Keywords: Water Treatment, Methylene Blue, Eosin Y, GO/ZnO, Adsorption, Pollution

INTRODUCTION

Water contamination has become one of the most serious problems across the globe since the advent of industrial revolution. As it is widely known, organic dyes cause serious water pollution because they are extensively used in the manufacturing of materials like dyestuff, ceramics, leather, and textiles; and are highly toxic, carcinogenic, and teratogenic. Discharging these dyes into the environment causes environmental pollution as well as serious life-threatening problems for human and aquatic organisms due to their high toxicity, low degradability, and high stability [1,2]. There are numerous effective methods to get rid of this form of pollution, and adsorption as a facile and economical method has been considered for this study. Researchers have made many efforts to develop and synthesize adsorbents that can eliminate contaminants from water. Due to their high stability, dyes are mostly resistant to light exposure and many other chemicals. Most of the dyes are injurious to humans and animals and cause many problems, such as eye burns by direct contact, difficulty in breathing by inhalation, and also vomiting and nausea if ingested [1].

Dyes are categorized into three classes: cationic, anionic, and non-ionic. Anionic dyes are acidic, direct, and very reactive, whereas cationic dyes are basic in nature [3]. MB is a cationic thiazine dye that is water-soluble, extremely hazardous and used for in production of leather, paper, and silk. Its excessive level may cause several diseases, like problems in respiratory and digestive systems [4,5]. EY is an anionic dye having bromine atoms and has been used in many areas including textile, printing, pigment, plastics, paper, dyestuffs, paint, leather, and dye-sensitized solar cells; its exposure can cause serious pollution due to its toxicity [6,7]. Therefore, it is necessary to remove these toxic and carcinogenic dyes from water to avoid the consequences of the effluents discharged and keep aquatic organisms and human beings safe.

To remove dyes from wastewater, mainly three techniques are used: chemical, biological, and physical methods. Chemical methods are advanced oxidation methods which include Fenton's reagent, electrocoagulation and solvent extraction method; biological methods use the species like bacteria, algae, and fungi for removal of dyes, whereas physical methods include ion exchange, filtration, coagulation and the adsorption process [8-10]. All the methods mentioned have some limitations: some are expensive while some have low efficiency. Only the adsorption method has been known as one of the most operative and prevalent treatments for removal of dyes from waste water because of its high efficiency and facileness; moreover, adsorbents can be easily recovered from the solution. It is considered to be the most operative and inexpensive treatment for removing pollutants from water. These properties make adsorption a favorable method for the removal of organic dyes from wastewater [11-13]. Adsorption is a very simple procedure that is defined

†To whom correspondence should be addressed.
E-mail: smokie@jejunu.ac.kr, gsiddiqi@jejunu.ac.kr

Table 1. Properties and structures of Eosin Y and methylene blue dyes

Dyes	EY	MB
Molecular formula	$C_{20}H_8Br_4O_5$	$C_{16}H_{18}N_3SCl$
Structure	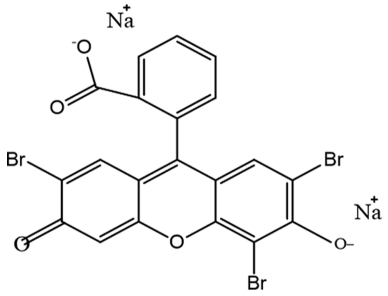	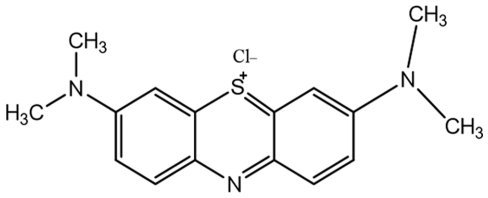
M. weight (g/mol)	647.89	319.85
C.I No	45,380	52,015
C.I name	Acid red 87	Basic blue 9
Melting point (°C)	295.5	100 to 110
λ max (nm)	517	664

as the accumulation of particles on a solid material's surface. It is a surface phenomenon that involves the application of surface forces. If there are adsorbable solutes (adsorbate) in a solution in contact with a solid (adsorbent) with an extremely porous surface structure, the adsorbate is then deposited on the adsorbent due to liquid-solid intermolecular forces of attraction [14].

Various types of adsorbents like activated carbon, alumina, titanium dioxide, peat, chitin, polymers, fungi, have been used to decontaminate waste water [1,4,15,16]. These adsorbents have certain drawbacks, such as activated carbon which is widely used as an adsorbent material of choice in many adsorption processes. However, considering the high cost and secondary pollution production of activated carbon and other such adsorbents, research is going on to grow low-cost substitute adsorbents [14]. Therefore, it is essential to use low priced and commercially available adsorbents for waste water purification [17]. Many researchers have focused their attention on graphene oxide (GO) based materials to remove contaminants from aqueous solutions [12,18,19]. GO is easily available, and has oxygen-containing functional groups which can easily interact with dyes and other contaminants present in aqueous solution. Similarly, zinc oxide (ZnO) has also been used as a good adsorbent for various dyes [20-24]. But most of these studies deal with only a single component dye solution and relatively few works discuss the adsorption of both cationic as well as anionic dyes by an adsorbent. Furthermore, the use of a composite of GO nanosheets and ZnO nanospheres (NSs) for the adsorption of both cationic and as well as anioni dyes is available in a very narrow range of literature.

In this study, GO nanosheets were synthesized by the modified Hummer's method, while ZnO NSs by co-precipitation method. Both the GO nanosheets and ZnO NSs were then mixed physically to form graphene oxide nanosheet-ZnO nanosphere nanocomposite. As-synthesized GO/ZnO nanocomposite was used as a highly effective adsorbent for the adsorption of both anionic (EY) and cationic (MB) dyes.

EXPERIMENTAL

1. Materials

All of the materials utilized were analytical grade reagents and used without further purification. Graphite powder, sodium nitrate ($NaNO_3$), potassium permanganate ($KMnO_4$), hydrogen peroxide (H_2O_2), concentrated sulfuric acid (H_2SO_4), zinc acetate dihydrate ($ZnAc_2$) ($C_4H_{10}O_6Zn$), anhydrous ethanol (C_2H_5OH,), n-hexane (C_6H_{14}), sodium hydroxide (NaOH), methylene blue and eosin y were purchased from Sigma-Aldrich. Some physical and chemical features of the EY and MB are given in Table 1.

2. Synthesis of GO Nanosheets

GO nanosheets were synthesized by modified Hummer's method. A 500 mL beaker was taken to which graphite powder (1.0 g) and 46 mL concentrated H_2SO_4 (97%) were added. The beaker was kept in an ice bath and stirred for 30 min. Then 1.0 g of $NaNO_3$ was added and stirred at 600 rpm for 2 h. After this 1.0 g of $KMnO_4$ was added while the beaker was still in the ice bath to keep the temperature lower than 20 °C to avoid overheating and stirred for another 2 h at the same rpm. After displacing from the ice bath, the temperature of the system was elevated to 35 °C and thoroughly stirred for 1 h at 600 rpm followed by dilution with deionized water (280 mL), and stirring was continued for a further 20 min. Then, the temperature was further increased to 95 °C with 30 minutes stirring and left for overnight stirring at room temperature; 6 mL of H_2O_2 was added dropwise till the dark brown color changed to yellow. The mixture was finally centrifuged at 1,500 rpm for 30 minutes to separate the solid products and then rinsed with deionized water multiple times till the pH was neutral. Finally, the residual was dried overnight at 60 °C to obtain GO nanosheets.

3. Synthesis of ZnO Nanospheres

ZnO NSs were synthesized through the alkaline co-precipitation method. In this method, 1.88 g of ZnAc2·2H_2O was added to 100 mL of anhydrous ethanol and refluxed for 4 h at 70 °C. Another

solution of 3 mmol NaOH in 10 mL anhydrous ethanol was prepared. This solution was then added into the ZnAc2·2H_2O solution and vigorously mixed followed by addition of N-hexane (20 mL) and left overnight. To obtain the precipitated ZnO NSs the solution was then centrifuged for 20 minutes. The synthesized NSs were washed three times with DI water to remove any impurities left and then allowed to dry.

4. Synthesis of GO/ZnO NSs Nanocomposite

For synthesizing the GO/ZnO nanocomposite the physical mixing method was adopted. In this method both the synthesized ZnO NSs and GO nanosheets are taken in 2 : 1, respectively, then mixed and ground to obtain the required nanocomposite.

5. Characterization

Bruker VECTOR-22 IR spectrometer was used to record FT-IR spectra of the samples. Zeta potential (ZP) of the samples was recorded at room temperature by a Zeta Sizer nano series (Malvern). Thermo Scientific Evolution 300 Spectrophotometer was used for UV-Visible absorbance measurements of the dyes. FESEM (TESCAN, MIRA3) was used for morphological characterization. X-ray diffraction analysis was performed through 151 PANanalytical's Empyrean XRD.

6. Adsorption Experiment

An adsorption study of anionic (EY) and cationic (MB) dyes onto the GO/ZnO NCs was conducted in a sequence of tests. In the single system, different concentrations of dyes were taken in vials; to this equal amount of GO/ZnO nanocomposite (3.0 mg/13 mL) was added to every vial and allowed to sonicate for 15 minutes. Then each vial was stirred at 300 rpm for 10 and 20 minutes in the case of EY and MB, respectively. To separate the solid and liquid phases, the suspension was centrifuged for 10 minutes at 15,000 rpm. The supernatant liquid was then analyzed by Thermo scientific evolution 300 UV-visible spectrophotometer for EY and MB by determining their absorbance at λ_{max}=517 and 664 nm, respectively.

For the binary dye system, one set of experiments was done at a fixed EY concentration of 100 mg/L, and MB concentration was changed from 10-40 mg/L. In the second set of experiments the MB concentration was kept constant at 40 mg/L and concentration of EY was changed in the range of 20-100 mg/L. Then the next steps were carried in accord with the above. When equilibrium was reached, the adsorption capacity and dye removal percentage were determined according to the following equations:

$$R\% = \frac{C_1 - C_2}{C_1} \times 100 \quad (1)$$

$$q_e = \frac{C_0 - C_e}{W} \times V \quad (2)$$

C_0 and C_e (mg/mL) are the concentrations of adsorbate at initial and equilibrium state. V is the liquid volume (mL), while W is the adsorbent dosage (g).

An equilibrium isotherm study is required to confirm the accuracy of our results, provide information about the reaction mechanism, and calculate the maximum adsorption capacity. A comparison of adsorption capacities of EY and MB using various adsorbents has been presented in Table 4. Similarly, adsorption kinetics studies are required to explore the governing mechanism of adsorption. Therefore, Langmuir and Freundlich isotherms and pseudo-first-order and pseudo-second-order kinetics were applied.

RESULTS AND DISCUSSION

1. Material Characterization

Fig. 1 shows the XRD results for the synthesized ZnO nanospheres and GO nanosheets. Fig. 1(a) is the XRD patterns of GO nanosheets, which exhibits two charasterictic peaks around 2θ= 24.86° and 2θ=42.3°, respectively. These patterns show mild oxidation of graphite to graphene oxide, as low quantity of $KMnO_4$ (1 g) was used for the oxidation [25]. The obtained diffraction pattern (Fig. 1(b)) is in good agreement with the standard JCPDS card for ZnO (No 36-1451), which corresponds to the wurtzite crystal structure of ZnO. The observed significant diffraction peaks and their corresponding crystal planes appeared at 30.2° (100), 32.8° (002), 34.6° (101), 45.8° (102), 54.9° (110), 57.6° (103), 61.3°

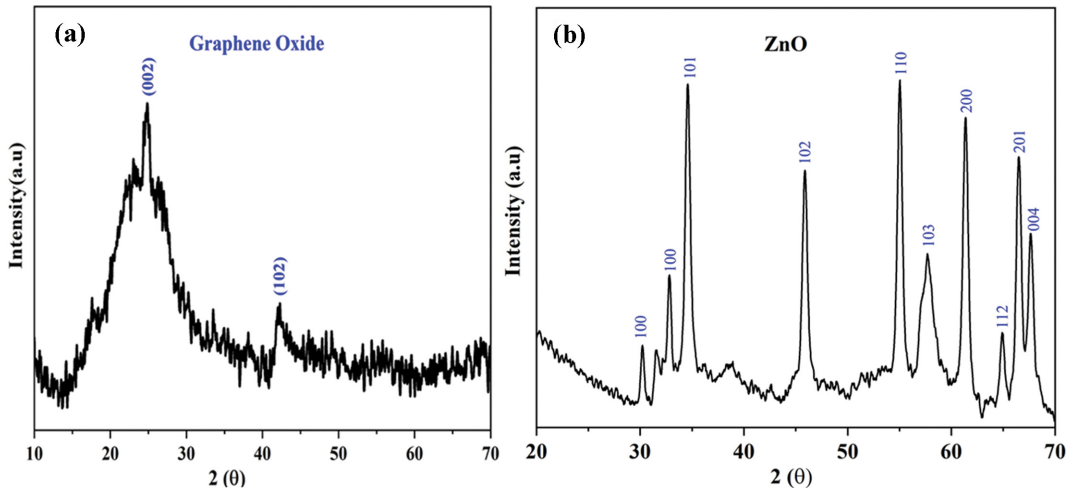

Fig. 1. (a) XRD spectra of graphene oxide nanosheets, (b) XRD patterns of ZnO showing wurtzite crystal structure.

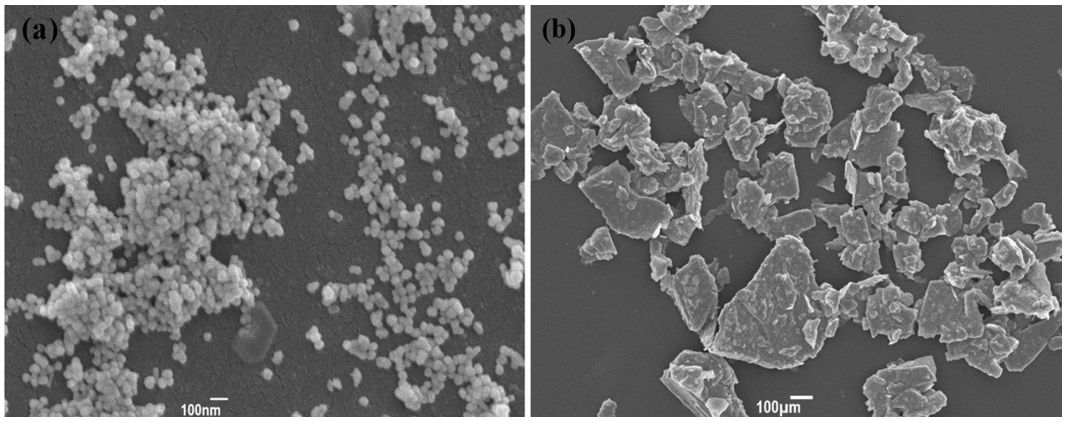

Fig. 2. (a) SEM image of zinc oxide showing homogeneity in shape and size, (b) SEM imges of graphene oxide nanosheets.

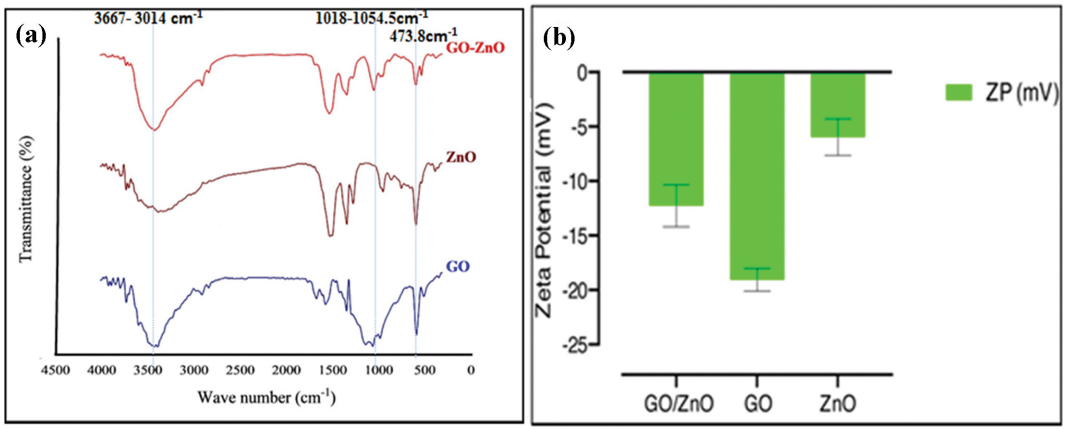

Fig. 3. (a) FTIR spectra of GO, ZnO, and GO/ZnO NC, (b) Zeta potential values showing the surface charge on surface of GO, ZnO, and GO/ZnO NCs.

(200), 64.9° (112), 66.4° (201) and 67.6° (004); all the diffraction peaks are in close agreement with the standard JCPDS data [26-28] and no characteristic peaks were observed other than ZnO, which shows that the ZnO nanospheres have no impurity.

Morphological characteristics of as synthesized ZnO NSs and GO nanosheets were analyzed by SEM as shown in Fig. 2. Fig. 2(a) represents the homogeneity in terms of shape, size and crystal structure of ZnO, as they did not represent the random orientation. A closer look at the SEM image reveals the presence of non-agglomerated single crystals of ZnO, identifying them as nanospheres. Fig. 2(b) shows the SEM image of GO nanosheets exfoliated by modified Hummer's method; it can be seen that they are well exfoliated to mono or few layers and their lateral size is from few micrometers to several nanometers.

FTIR spectra of GO nanosheets, ZnO NSs, and GO/ZnO NCs are given in Fig. 3(a). For GO the following characteristic bands appeared: Carbonyl (C=O) at a wavenumber of 1,723 cm^{-1}, carbon-carbon double bond (C=C) at 1,628 cm^{-1}, a broad band from 3,667.09-3,014.6 cm^{-1}, for hydroxyl groups where the hydroxyl groups may be incorporated from phenolic OH or from absorbed water molecules or OH from carboxylic groups; the peaks at 2,929.9 and 2,858.1 cm^{-1}, are due to the CH_2 stretching and antisymmetric vibration. The peak at 1,406.8 cm^{-1} is because of the C-O bond of COOH, while the peaks at 1,204.5, 1,131.4, and 1,054.5 cm^{-1} are due to aliphatic C-O and epoxy C-O stretching, respectively. For ZnO NSs the peaks at 3,691.4-2,919.2 cm^{-1}, are because of the OH stretching vibration, the peaks at 2,880.00 and 2,816.43 cm^{-1}, are due to aliphatic CH stretching of alkane, 1,583.4 and 1,400.2 cm^{-1}, are due to zinc carboxylate bond stretching, 1,018.83 cm^{-1}, is due to C-O bond stretching, and the peak at 473.8 cm^{-1}, is due Zn-O bond. Comparing the spectra of GO- ZnO nanocomposite with that of GO and ZnO shows a slight shift with the change in intensity of O-H peaks at 3,675-2,960 cm^{-1}. Besides, the peaks for carbonyl disappeared in the composite, which confirms the formation of GO-ZnO nanocomposite.

The ZP values of ZnO NSs, GO nanosheets, and GO/ZnO NCs are shown in Fig. 3(b). DI water having pH 6.8 was used for preparing the solutions to measure ZP values. The average ZP values for, ZnO NSs, GO nanosheets and GO/ZnO nanocomposite are −5.96, −19.066, and −12.26 mV, respectively. The negative value of zeta potential shows the repulsion and stability of the particles. The movement of nanoparticles is used to determine zeta potential under the influence of applied electric field. The surface charge as well as the local environment of the nanoparticles influence their mobility.

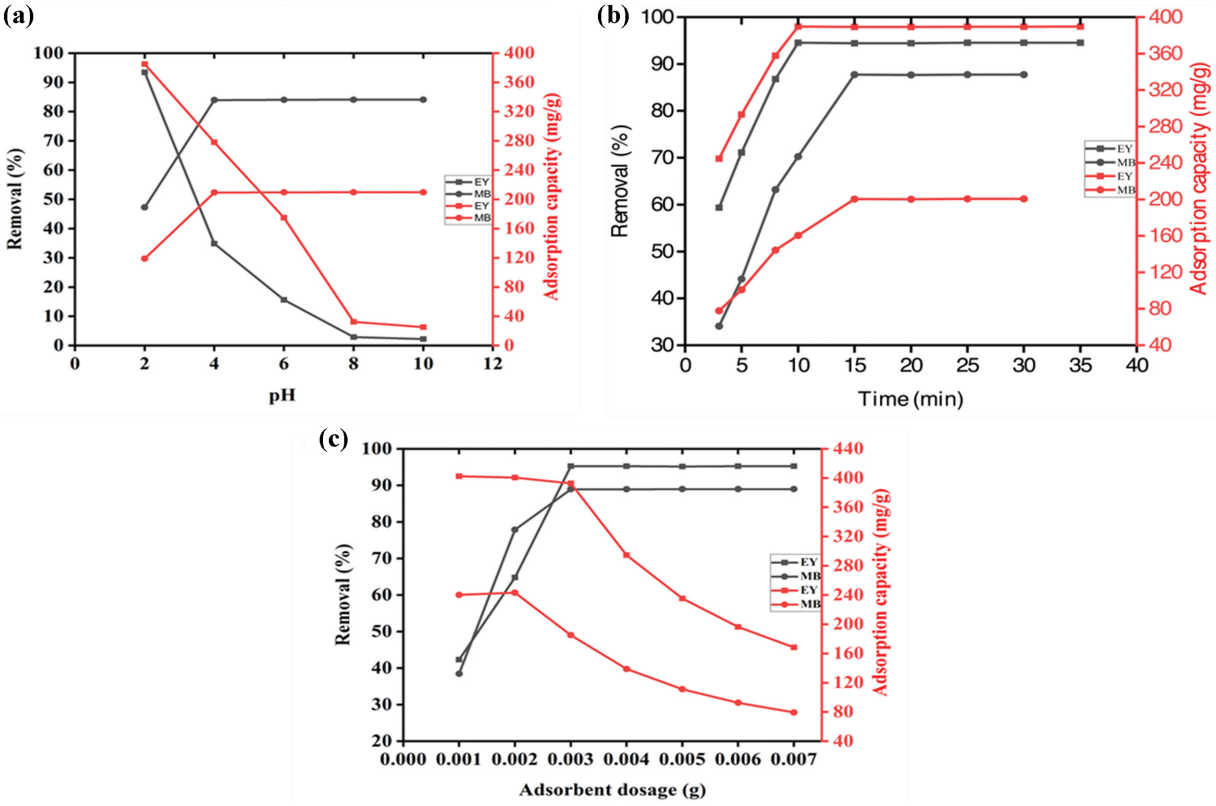

Fig. 4. Effect of (a) pH, (b) Time, (c) dosage of adsorbent on adsorption of EY and MB dyes by GO/ZnO-NCs.

2. Adsorption Study of EY and MB in a Single Solution

2-1. Effect of pH of Solution on the Removal of Dyes

The pH of the solution highly affected the adsorption efficiency of dyes onto the adsorbent. Therefore, for further investigation, the optimum pH value was important [29]. The influence of pH from 2.0 to 10.0 on the equilibrium adsorption capacity of both dyes was investigated using 0.1 mol/L HCl and NaOH solution for adjusting pH, with the concentrations of EY at 100 mg/L and MB at 40 mg/L. Fig. 4(a) displays the adsorption behavior of EY and MB at different pH values. At lower pH, a larger adsorption capacity (384.9793 mg/g) (with 0.230 g mass loading) (3.0 mg/13 mL) was observed for EY, whereas on increasing pH the adsorption capacity decreased. The reason for this behavior is that at lower pH, the surface of GO/ZnO nanocomposite was severely protonated and the negatively charged dye was easily attracted to the positively charged adsorbent. Whereas, with an increase in pH the adsorbent became negatively charged, due to which the negatively charged EY molecules may have been repelled away from its surface because of the electrostatic repulsion and hence the adsorption capacity decreased. Therefore, an acidic condition (pH=2) was implemented for further experiments.

For MB the adsorption capacity of GO/ZnO NCs increased with the increasing pH of the solution. At lower values of pH, hydrogen ions competed with MB cation due to which adsorption capacity was reduced, whereas at higher pH values negative charge appeared on the surface of adsorbent, which favored electrostatic attraction and adsorption amount for the positively charged MB molecules. The optimum pH was predicted to be pH 6 at which a maximum adsorption capacity of ≈210 mg/g was detected.

2-2. Effect of Contact Time on Dyes Removal.

Fig. 4(b) displays the effect of contact time on the adsorption of EY and MB by GO/ZnO NCs. The contact time varied in the range of 2-35 min. The rate of adsorption of EY and MB was rapid initially, and this was because of the larger surface area and higher amount of available active sites on the adsorbent surface [6]. Afterwards, the adsorption rate slowed and became stagnant and finally attained equilibrium. This is because all the active sites were occupied by dye molecules. The equilibrium time was 10 and 15 min for EY and MB, respectively.

2-3. Effect of Adsorbent Dosage on Dyes Removal

The effect of adsorbent dosage on adsorption was investigated by adding an amount of GO/ZnO in the range of 1.0-7.0 mg into the vials having 13 mL of 100 mg/L EY and 40 mg/L MB solution at pH=2 and 6 for EY and MB, respectively; the results are given in Fig. 4(c). Percentage removal of EY and MB by adding GO/ZnO increased from 42.30% to 95.24% and 38.45% to 88.71%, respectively, as the adsorbent amount increased up to 3.0 mg and then remained constant for both dyes. The increase in removal percentage of dyes with an increasing amount of adsorbent in the initial stage could be owing to the better availability of active sites on the surface of the adsorbent, which could accelerate the accessibility of adsorbate molecules. Contrary to the removal percentage, the adsorption capacity decreased as the adsorbent dosage was increased. This was because, at a larger amount of adsorbent, the accessibility of high energy adsorbent active sites was reduced, and a larger portion of active sites having lower energy were occupied due to

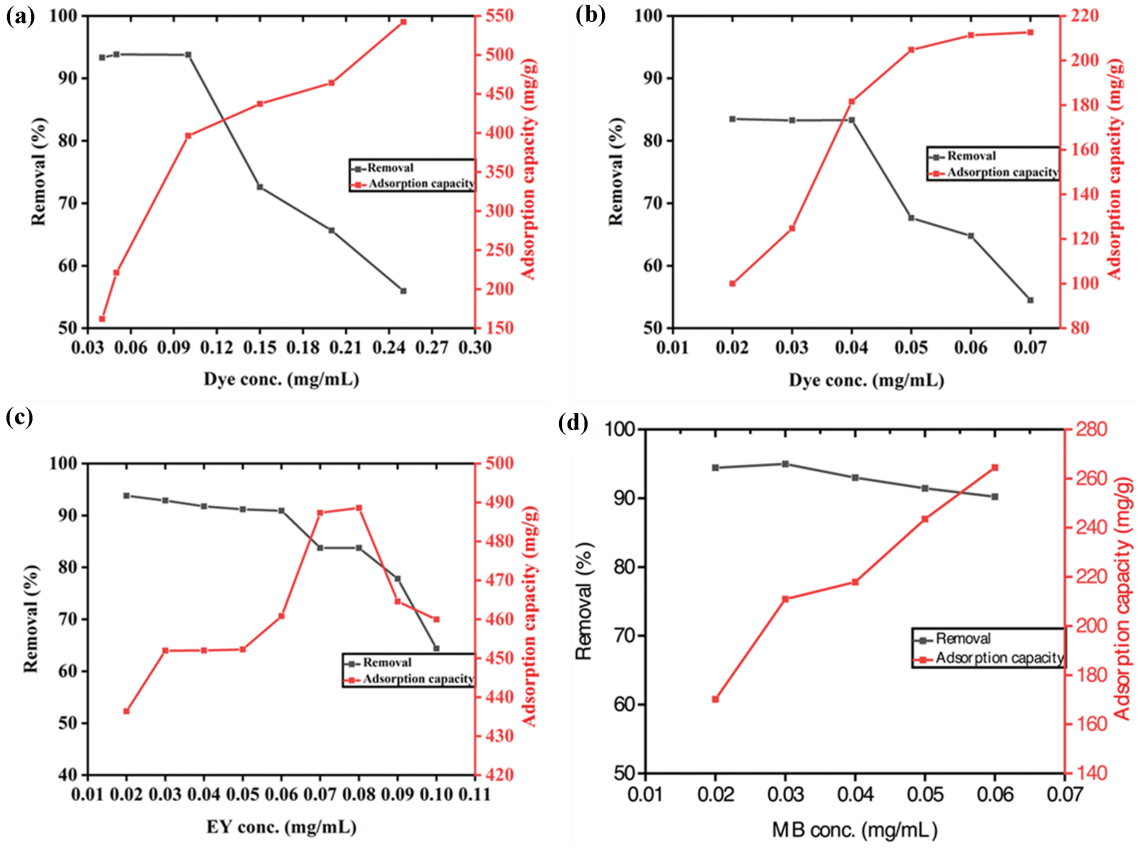

Fig. 5. (a) Effect of initial dyes concentration of EY (b) MB (c) Effect of MB (C_0=40 mg/L) on the removal of EY by GO/ZnO (d) Effect of EY (C_0=100 mg/L) on the removal of MB by GO/ZnO.

which adsorption capacity decreased [24]. As a result, the amount of 3.0 mg of adsorbent/13 mL dyes solution was chosen for further study.

2-4. Effect of Initial Concentration of Dyes

To investigate the effect of the initial concentration of dye, the concentration of EY and MB varied from 50 to 250 mg/L and 20 to 70 mg/L, as indicated in Fig. 5(a) and 5(b), respectively. At lower concentrations (40-100 mg/L for EY) and (20-40 mg/L for MB), the removal efficiency of both dyes was 93% and 83%, respectively. However, a decrease in adsorption efficiency was observed by further increasing the concentration of the dyes. This difference can be described by the statement that at a lesser concentration of dyes, the sites for adsorption are available in excess, but as the concentration of dyes increases the ratio of sites on the adsorbent is comparatively reduced, for the available dye molecules were saturated easily because of the high concentration of dyes.

In contrast to removal efficiency, the adsorption capacity of the adsorbent increased for both (EY and MB) dyes in accord with an increase in the concentration of solutions. This increase is due to the high availability of dye molecules in the surrounding of the adsorbent and the extraordinary driving potential of the bulk transfer before reaching the adsorption-desorption equilibrium [30-32].

2-5. Adsorption of Cationic-anionic Dyes in Binary Dye Solutions

Fig. 5(c) and 5(d) show the co-adsorption of a mixture of both EY and MB dyes, and this study was carried out because it is more important from a practical point of view. In one binary solution, the concentration of EY was fixed at 100 mg/L, while that of MB was varied from 20-60 mg/L, as given in Fig. 5(d). The removal percentage and adsorption capacity of MB was greater than in the single MB dye solution by GO/ZnO nanocomposite, while in the second binary solution the MB concentration was kept fixed at 40 mg/L and that of EY was changed in the range of 20-100 mg/L. For GO/ZnO nanocomposite the percentage removal and adsorption capacity of EY in the presence of MB was also superior to the single EY dye solution. It was observed that both EY and MB adsorption increased in the binary solutions, which revealed that the co-adsorption of dyes showed a synergistic effect, not competitive adsorption.

3. Kinetics Study

Kinetics is an essential step in studying the adsorption process. It allows us to estimate the adsorption rates and rate expressions of the possible reaction mechanism, so the pseudo-first-order and second-order kinetics were studied. These two models are given in linear form as follows [33].

$$\mathrm{Log}(q_e - q_t) = \log q_e - \frac{k_1}{2.303} \times t \tag{3}$$

$$\frac{t}{q_t} = \frac{1}{k_2 q_e^2} + \frac{t}{q_e} \tag{4}$$

where q_e and q_t are the amounts in (mg/g) of dyes adsorbed at equilibrium and any time (min), respectively. K_1 (min^{-1}) is the pseudo-

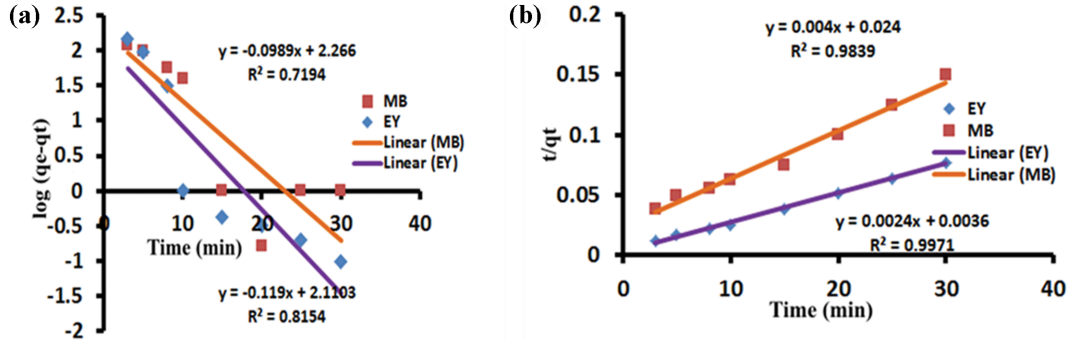

Fig. 6. (a) pseudo-first order EY and MB. (b) pseudo-second order for EY and MB.

Table 2. Kinetic parameters of EY and MB adsorption on GO/ZnO nanocomposite

Dye	Pseudo-first order				Pseudo-second order		
	q_e (exp) mg/g	K_1 min^{-1}	R^2	q_e (cal.) mg/g	K_2 g/mg/min	R^2	q_e (cal) mg/g
EY	384	0.274057	0.8154	8.250716	0.0016	0.9971	416.6667
MB	210	0.227767	0.7194	9.640761	0.000667	0.9839	250

first-order rate constant, while k_2 (g/mg min) is the pseudo-second-order rate constant. The intercept and slope of the plot of t/q_t against t were used to find the values of k_2 and q_e as given in Fig. 6(b), while the results are given in Table 2. The R^2 values of 0.9971 for EY and 0.9839 for MB of pseudo-second-order kinetics were greater than the first-order. The q_e (cal.) values of of the pseudo-second-order kinetic model for both EY and MB are closer to q_e (exp) values when compared to the values obtained from the first order. It suggests that the adsorption followed the pseudo-second-order kinetics rather than pseudo-first-order.

4. Isotherm Study

The equilibrium relationship and the interaction between the adsorbent and adsorbate solution can be described using the isotherms of adsorption [34]. In this study the popular isotherms, namely Freundlich and Langmuir, were explored to decide the best model for dye adsorption. The assumption of Langmuir model is that adsorption occurs on the homogeneous surface of the adsorbent, while the adsorbate forms a monolayer on its surface with uniform energy of adsorption. The Freundlich model, on the other hand, suggests that adsorption occurs in a multilayer manner on a heterogeneous surface with non-uniform affinities over the heterogeneous surface as well as non-uniform distribution of adsorption heat [32]. The following equations are used to express both these models:

$$\frac{C_e}{q_e} = \frac{1}{k_L q_m} + \frac{C_e}{q_m} \tag{5}$$

$$\ln q_e = \ln K_f + \frac{1}{n} \ln C_e \tag{6}$$

where q_e (mg/g) is the adsorbate adsorbed per unit mass of the adsorbent, C_e (mg/L) represents the concentration of dyes at equilibrium, K_L (L/mg) and q_m (mg/g) are the Langmuir adsorption constants representing the heat of adsorption and monolayer adsorption capacity, respectively.

K_f (mg/g (L/mg) 1/n), the Freundlich constant, denotes the adsorption capacity, and n is called the heterogeneity factor, which is related to the multilayer adsorption intensity representing the adsorption feasibility. Slopes and intercepts of the plot of C_e/q_e versus C_e and $\ln q_e$ versus $\ln C_e$ were used to calculate the Langmuir constants and Freundlich parameters as given in Fig. 7(a) and (b), respectively. Table 3 represents the calculated parameters. Looking

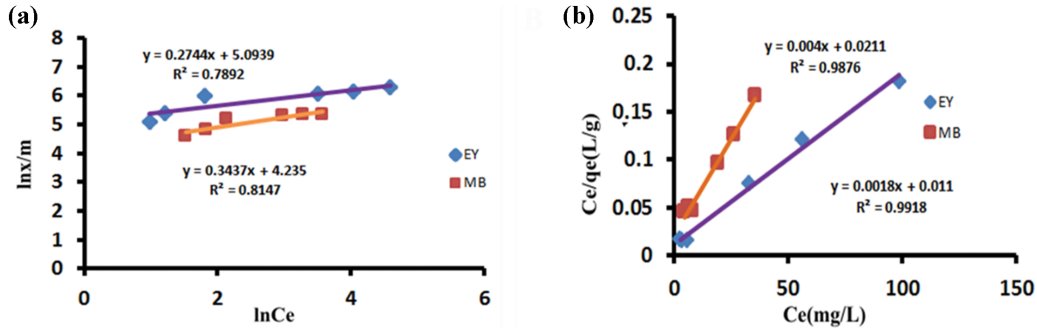

Fig. 7. (a) Freundlich and (b) Langmuir isotherm for EY and MB.

Table 3. Langmuir and Freundlich isotherm constants for EY and Mb adsorption on GO/ZnO nanocomposite

Dye	Langmuir				Freundlich		
	$q_{e(exp)}$ mg/g	K_L L/mg	R^2	$q_{(max)}$ mg/g	K_f mg/g	R^2	1/n
EY	384	0.163636364	0.9918	555.55	163.0244	0.7892	0.2744
MB	210	0.189573	0.9876	250	69.06168	0.8147	0.3437

Table 4. Comparison of adsorption capacities of various adsorbents for the removal of EY and MB from aqueous solutions

Adsorbents	q_m (mg/g)		Ref.
	MB	EY	
Lala Clam (Orbicularia orbiculata) Shell	9.61		5
Coffee and peanut husk modified with magnetite iron oxide nanoparticles	88.49		1
ZnO nanoparticles	190		23
platinum-doped titanate nanomaterials	122.1		35
Reduced graphene oxide	121.95		33
Fe-Mn binary oxide nanoparticles:	72.32		36
$MgFe_2O_4$/reduced graphene oxide nanoparticles	24.81		37
Cu (OH)2-nanoparticle loaded activated carbon:	32.9	26.4	38
Ferroferric oxide/polypyrrole magnetic composite		212.31	7
Chitosan hydro beads		76	39
Iron sulfide functionalized polyaniline nanocomposite		48.72	40
Silver-graphene oxide nanocomposite		256.41	41
Biosorbent based on sugarcane bagasse modified with tetraethylenepentamine		399	42
Porous carbon prepared from tea waste		400	43
Graphene oxide nanosheets		217.33	6
Zinc oxide nanoparticles loaded on activated carbon		163.9	44
Graphene oxide-zinc oxide nanocomposite	250	555.55	This study

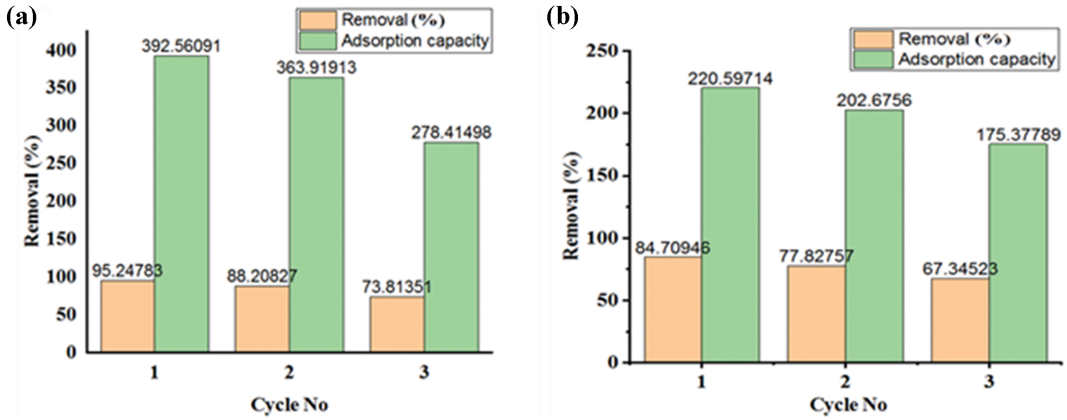

Fig. 8. Reusability of GO/ZnO NCs for (a) EY (b) MB.

at the correlation coefficients (R^2) values of (0.9918) for EY and 0.9876 for MB of Langmuir isotherm are greater than those deduced from the Freundlich model, which specify that the adsorption of EY and MB on GO/ZnO NCs fitted well with Langmuir isotherm and took place in a monolayer fashion.

5. Reusability of GO/ZnO NCs

Reusability of the adsorbent is an important factor from a practical point of view. For desorption of both EY and MB dyes from GO/ZnO NCs, 0.1 M NaOH and HCl were used, respectively. Once the dyes were desorbed the GO/ZnO NCs were washed with deionized water, then dried and again used for the adsorption of EY and MB up to three consecutive cycles. The results for the reusability of GO/ZnO NCs for EY and MB are given in Fig. 8(a) and (b), respectively. In the first cycle the removal percentage of EY observed was 95.24%, whereas the adsorption capacity calculated was 392.56 mg/g. In the second and third cycles the removal percentage decreased to 88.20% and 73.81%, respectively, while the adsorption capacity dropped to 363.91 and 278.41 mg/g.

For MB the removal percentage and adsorption capacity were 84.70% and 220.59 mg/g, respectively, in the first cycle. While in

the second and third cycles the removal percentage was reduced to 77.82% and 67.34%, respectively, whereas the adsorption capacity decreased to 202.67 and 175.37 mg/g. The gradual decrease in removal percentage and adsorption capacities up to three cycles suggests that GO/ZnO NCs can be reused for adsorption of dyes from industrial wastewater and can be applied as an effective and economical adsorbent.

CONCLUSIONS

Nanocomposites of graphene oxide nanosheets and zinc oxide nanospheres were synthesized and characterized by XRD, SEM, FT-IR, DLS and were successfully applied as an excellent adsorbent material for the removal of MB and EY from aqueous solution. The adsorption data for both dyes fitted well with the Langmuir isotherm with a maximum monolayer adsorption capacity of 555 and 250 mg/g of the adsorbent for EY and MB, respectively. The kinetic study showed that the adsorption followed a pseudo-second-order model. The as-prepared nanocomposite possessed a high surface area and showed better adsorption ability for both dyes. In a binary system, the adsorption capacity for both dyes was better than the single dye solution. These results demonstrate that this nanocomposite can be used as an excellent and low-cost adsorbent for removal of both anionic as well as cationic dyes from an aqueous solution, which may have remarkable potential in waste water treatment application.

ACKNOWLEDGEMENTS

This research was funded by "H.E.J. Research Institute of Chemistry, ICCBS, University of Karachi, Brain Pool program (2021H1 D3A2A02039269) and Basic Science Research Program (2021R1 A2C2011441& 2021R1A4A2000934) funded by the Ministry of Science and ICT through the National Research Foundation of Korea".

REFERENCES

1. N. Besharati, N. Alizadeh and S. Shariati, *J. Mex. Chem. Soc.*, **62**, 110 (2019).
2. A. Salama, K. R. Shoueir and H. A. Aljohani, *Fibers Polym.*, **18**, 1825 (2017).
3. S. Sharma, R. Saxena and G. Gaur, *IOSR J. Appl. Chem.*, **7**, 6 (2014).
4. S. Yadav, A. Asthana, R. Chakraborty, B. Jain, A. K. Singh, S. A. Carabineiro, M. Susan and M. A. B. H. Susan, *Nanomaterials*, **10**, 170 (2020).
5. A. A. A. Eljiedi and A. Kamari, *AIP Conf. Proc.*, **1847**, 040003 (2017).
6. P. Veerakumar, J. Tharini, M. Ramakrishnan, I. Panneer Muthuselvam and K.-C. Lin, *ChemistrySelect*, **2**, 3598 (2017).
7. M. Zhang, Z. Yu and H. Yu, *Polym. Bull.*, **77**, 1049 (2020).
8. S. Sharma and A. Kaur, *Indian J. Sci. Technol.*, **11**, 1 (2018).
9. K. Kalantari, M. Kalbasi, M. Sohrabi and S. J. Royaee, *Ceram. Int.*, **42**, 14834 (2016).
10. I. Khurana, A. Saxena, Bharti, J. M. Khurana and P. K. Rai, *Water, Air, Soil Pollut.*, **228**, 180 (2017).
11. M. Fathy, T. Abdel Moghny, M. A. Mousa, A. H. A. A. El-Bellihi and A. E. Awadallah, *Appl. Nanosci.*, **6**, 1105 (2016).
12. Y. Cao and X. Li, *Adsorption*, **20**, 713 (2014).
13. F. Zhang, J. Lan, Y. Yang, T. Wei, R. Tan and W. Song, *J. Nanopart. Res.*, **15**, 2034 (2013).
14. R. V. Kandisa, K. V. N Saibaba, K. B Shaik and R. Gopinath, *J. Bioremediat. Biodegrad*, **7**, 371 (2016).
15. A. G. Cordova, M. D. P Morales and E. Mazario, *Water*, **11**, 2372 (2019).
16. S. Bhattacharya, I. Saha, A. Mukhopadhyay, D. Chattopadhyay and U. Chand, *Int. J. Chem. Sci. Technol.*, **3**, 59 (2013).
17. S. Sivamani and G. B. Leena, *Int. J. Biosci. Technol.*, **2**, 47 (2009).
18. J. Liang, Y. Huang, F. Zhang, Y. Zhang, N. Li and Y. S. Chen, *Sci. China Technol. Sci.*, **57**, 284 (2014).
19. S. Liu, J. Ma, W. Zhang, F. Luo, M. Luo, F. Li and L. Wu, *J. Radioanal. Nucl. Chem.*, **306**, 507 (2015).
20. S.-W. Bian, I. A. Mudunkotuwa, T. Rupasinghe and V. H. Grassian, *Langmuir*, **27**, 6059 (2011).
21. A. Atta, M. A. Akl, A. M. Youssef and M. A. Ibraheim, *Adsorpt. Sci. Technol.*, **31**, 397 (2013).
22. M. O. Fatehah, H. A. Aziz and S. Stoll, *J. Colloid Sci. Biotechnol.*, **3**, 75 (2014).
23. J. C. Kulkarni, A. Chavhan, A. Bappakhane and J. Chimmankar, *Rjces*, **4**, 158 (2016).
24. M. N. Zafar, Q. Dar, F. Nawaz, M. N. Zafar, M. Iqbal and M. F. Nazar, *J. Mater. Res. Technol.*, **8**, 713 (2019).
25. K. Krishnamoorthy, M. Veerapandian, K. Yun and S.-J. Kim, *Carbon N.Y.*, **53**, 38 (2013).
26. J. Xia, K. Diao, Z. Zheng and X. Cui, *RSC Adv.*, **7**, 38444 (2017).
27. K. Vidhya, M. Saravanan, G. Bhoopathi, V. P. Devarajan and S. Subanya, *Appl. Nanosci.*, **5**, 235 (2015).
28. A. Sagasti, N. Bouropoulos, D. Kouzodis, A. Panagiotopoulos, E. Topoglidis and J. Gutierrez, *Materials*, **10**, 849 (2017).
29. C. Sarkar, C. Bora and S. K. Dolui, *Ind. Eng. Chem. Res.*, **53**, 16148 (2014).
30. M. W. Ashraf, N. Abulibdeh and A. Salam, *Int. J. Chem. Eng.*, **2019**, 1 (2019).
31. S. Saber-Samandari, S. Saber-Samandari, H. Joneidi-Yekta and M. Mohseni, *Chem. Eng. J.*, **308**, 1133 (2017).
32. Z. Monsef Khoshhesab and S. Souhani, *J. Chinese Chem. Soc.*, **65**, 1482 (2018).
33. F. A. Arias, M. Guevara, T. Tene, P. Angamarca, R. Molina, A. Valarezo, O. Salguero, C. V. Gomez, M. Arias and L. S. Caputi, *Nanomaterials*, **10**, 681 (2020).
34. B. Boukoussa, A. Hakiki, S. Moulai, K. Chikh, D. E. Kherroub, L. Bouhadjar, D. Guedal, K. Messaoudi, F. Mokhtar and R. Hamacha, *J. Mater. Sci.*, **53**, 7372 (2018).
35. C. H. Nguyen and R. S. Juang, *J. Taiwan Inst. Chem. Eng.*, **99**, 166 (2019).
36. K. Lu, T. Wang and L. Zhai, *J. Colloid Interface Sci.*, **539**, 553 (2019).
37. M. Adel, M. A. Ahmed and A. A. Mohamed, *J. Phys. Chem. Solids*, **149**, 109760 (2021).
38. S. Dashamiri, M. Ghaedi, A. Asfaram, F. Zare and S. Wang, *Ultrason. Sonochem.*, **34**, 343 (2017).
39. S. Chatterjee, S. Chatterjee, B. P. Chatterjee and A. R. Das, *J. Colloid Interface Sci.*, **288**, 30 (2005).
40. B. Y. Danu, E. S. Agorku, F. K. Ampong, J. A. M. Awudza and V.

Torve, *Polym. Sci.*, **63**, 304 (2021).
41. T. Jeyapragasam, *Mater. Today Proc.*, **3**, 2146 (2016).
42. G. B. Jiang, Z. T. Lin, X. Y. Huang, Y. Q. Zheng, C. C. Ren, C. K. Huang and Z. J. Huang, *Int. J. Biol. Macromol.*, **50**, 707 (2012).
43. L. Borah, M. Goswami and P. Phukan, *Biochem. Pharmacol.*, **3**, 1018 (2015).
44. Y. Rashtbari, S. Afshin and A. Hamzezadeh, *Environ. Sci. Pollut. Res.*, **29**, 5194 (2022).